A comparison between the effects of artificial land cover and anthropogenic heat on a localized heavy rain event in 2008 in Zoshigaya, Tokyo, Japan

Kazuyoshi Souma,[1] Kenji Tanaka,[2] Tadashi Suetsugi,[1] Kengo Sunada,[1] Kazuhisa Tsuboki,[3] Taro Shinoda,[3] Yuqing Wang,[4] Atsushi Sakakibara,[5] Koichi Hasegawa,[5] Qoosaku Moteki,[6] and Eiichi Nakakita[2]

Received 1 July 2013; revised 16 September 2013; accepted 17 September 2013; published 29 October 2013.

[1] On 5 August 2008, a localized heavy rainfall event caused a rapid increase in drainpipe discharge, which killed five people working in a drainpipe near Zoshigaya, Tokyo. This study compared the effects of artificial land cover and anthropogenic heat on this localized heavy rainfall event based on three ensemble experiments using a cloud-resolving model that includes realistic urban features. The first experiment CTRL (control) considered realistic land cover and urban features, including artificial land cover, anthropogenic heat, and urban geometry. In the second experiment NOAH (no anthropogenic heat), anthropogenic heat was ignored. In the third experiment NOLC (no land cover), urban heating from artificial land cover was reduced by keeping the urban geometry but with roofs, walls, and roads of artificial land cover replaced by shallow water. The results indicated that both anthropogenic heat and artificial land cover increased the amount of precipitation and that the effect of artificial land cover was larger than that of anthropogenic heat. However, in the middle stage of the precipitation event, the difference between the two effects became small. Weak surface heating in NOAH and NOLC reduced the near-surface air temperature and weakened the convergence of horizontal wind and updraft over the urban areas, resulting in a reduced rainfall amount compared with that in CTRL.

Citation: Souma, K., et al. (2013), A comparison between the effects of artificial land cover and anthropogenic heat on a localized heavy rain event in 2008 in Zoshigaya, Tokyo, Japan, *J. Geophys. Res. Atmos.*, *118*, 11,600–11,610, doi:10.1002/jgrd.50850.

1. Introduction

[2] In recent years, localized heavy rainfall events over urban areas have caused severe damage in Japan. Although localized heavy rainfall events produce low total rainfall amount, they can produce very intense rainfall in a limited area and in a short time period. Intense rainfall in urban river basins with small catchments and impervious land cover can cause inundation of areas inside levees and increase river channel and drainage pipe water levels rapidly. For example, the severe localized heavy rainfall that occurred near Zoshigaya, Tokyo, on 5 August 2008, caused a rapid increase in discharge and killed five people working in a drainage pipe.

[3] To improve the skill of numerical weather prediction, considerable efforts have been made to data assimilation to improve the initial conditions of numerical forecast models [e.g., *Kawabata et al*., 2007]. Urban canopy models used in cloud-resolving models are also being improved [e.g., *Tanaka and Ikebuchi*, 1994; *Kusaka et al*., 2001; *Kusaka and Kimura*, 2004; *Tanaka*, 2004; *Kanda et al*., 2005; *Lei et al*., 2008].

[4] *Pielke et al*. [2007, 2011] indicated that the urbanization is one of the important issues for the impacts of land use and land cover on local, mesoscale, and regional climate, including rainfall. The Metropolitan Meteorological Experiment conducted in St. Louis, MO, USA, in 1970, showed that urban conditions led to increased precipitation during summer [e.g., *Changnon and Huff*, 1986; *Shepherd*, 2005]. *Shepherd and Burian* [2003] indicated that rainfall has increased downwind of Houston, Texas, using data derived from the precipitation radar onboard the Tropical Rainfall Measuring Mission. *Niyogi et al*. [2010] indicated that thunderstorms occurred more frequently over Indianapolis, IN, USA, than over a rural area based on an analysis of the radar-based climatology of 91 summertime thunderstorm cases from 2000 to 2009.

[1]Interdisciplinary Graduate School of Medicine and Engineering, University of Yamanashi, Kofu, Japan.
[2]Disaster Prevention Research Institute, Kyoto University, Uji, Japan.
[3]Hydrospheric Atmospheric Research Center, Nagoya University, Nagoya, Japan.
[4]International Pacific Research CenterSchool of Ocean and Earth Science and Technology, University of Hawaii at Manoa, Honolulu, Hawaii, USA.
[5]ChudenCTI Co., Ltd, Nagoya, Japan.
[6]Research Institute for Global Change, Japan Agency for Marine-Earth Science and Technology, Yokohama, Japan.

Corresponding author: K. Souma, Interdisciplinary Graduate School of Medicine and Engineering, University of Yamanashi, 1F7 Kogyo-kaikan, 4-3-11 Takeda, Kofu, Yamanashi 400-8511, Japan. (ksohma@yamanashi.ac.jp)

2169-897X/13/10.1002/jgrd.50850

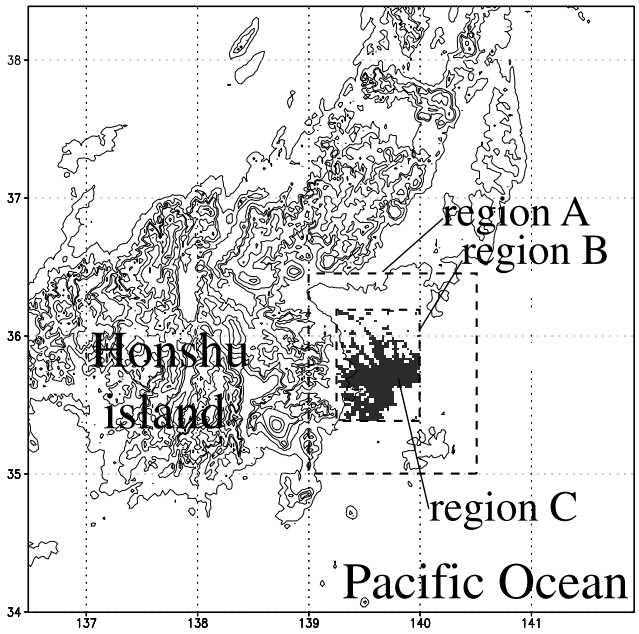

Figure 1. Model domain (with 2 km horizontal resolution and 45 vertical layers) and analysis regions. The thin black contours indicate terrain heights of 100, 500, 1000, and 2000 m, and the thick black contour shows the terrain height of 0 m. Region C was defined as the area in region B in which the fraction of urban area within the 2 km grid cell exceeds 30%.

Kishtawal et al. [2009] found that the increasing trend in the frequency of observed heavy rainfall events over Indian monsoon region is more likely in regions where the pace of urbanization is faster, by using in situ and satellite-based precipitation and population data sets. In the Tokyo metropolitan area, Japan, observational studies have also suggested that the urbanization affects summer rainfall, including localized heavy rainfall. In an analysis of 16 year Automated Meteorological Data Acquisition System (AMeDAS) rain gage data, *Fujibe* [1998] found a positive precipitation anomaly related to the urban effect over the central and inland areas of Tokyo. *Sato et al*. [2006] found that the precipitation frequency in the metropolitan area in and around Tokyo was remarkably higher than that in the surrounding areas based on an analysis of 12 year radar data.

[5] Some researchers have attempted to investigate the effect of urban areas on localized heavy rainfall based on numerical model experiments. *Gero and Pitman* [2006] reported that the size of the urban area on the western plain of central Taiwan affected the location of thunderstorms and precipitation. *Shem and Shepherd* [2009] indicated that the existence of urban areas contributed to the intensification of convective rainfall systems in two rainfall events over Atlanta, GA, USA. *Shepherd et al*. [2010] indicated that future growth of urban land cover could cause an expansion of heavy rainfall area over Houston, Texas. *Niyogi et al*. [2010] showed that a typical storm over Indianapolis was greatly affected by the existence of an urban area.

[6] Focusing on the Tokyo metropolitan area, *Kanda et al*. [2001] carried out numerical simulations for a cumulus cloud line over a major street in Tokyo under summer conditions and showed that the cloud line weakened and shifted toward a suburban area without urban heating. *Moteki et al*. [2005] found that the existence of the urban area intensified a convective rainfall event occurred in Tokyo in 1999. *Matheson and Ashie* [2008] identified different urban effects on precipitation based on numerical experiments for several rainfall events in Tokyo.

[7] Although the impact of the urban heat island on precipitation over and leeward and windward of cities has been studied using numerical models, most of them have focused mainly on the existence of a city, based on sensitivity experiments with the city artificially replaced by grassland or forest. The influences of urban areas on the urban heat island and precipitation include the effects of anthropogenic heat, artificial land cover, and three-dimensional urban geometry [e.g., *Ryu and Baik*, 2012]. To appropriately improve numerical weather predictions and apply the results to mitigation policies in urban planning, the impacts of urban on both momentum exchange and heat transfer need to be assessed separately. In addition, there is a need to understand how individual components of the urban environment may affect precipitation.

[8] Urban environmental components that may affect heat transfer include anthropogenic heat from devices, such as air conditioners and automobiles, and artificial land cover, such as asphalt. Particularly, artificial changes in land cover and land use simultaneously modify momentum transfer. So far, few studies have attempted to understand the individual effects of artificial land cover and anthropogenic heat on precipitation in urban areas. Artificial land cover on one hand suppresses surface evaporation and on the other hand converts incoming solar energy to surface sensible heat.

[9] With the aforementioned considerations, in this study we conducted ensemble experiments using a cloud-resolving

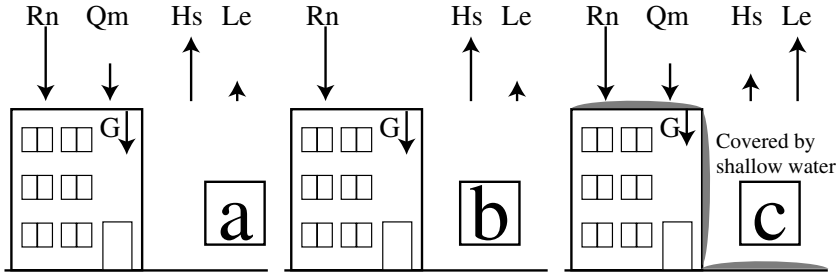

Figure 2. Schematic diagram showing the heat budgets for the land surface in three ensemble simulations: (a) CTRL, (b) NOAH, and (c) NOLC.

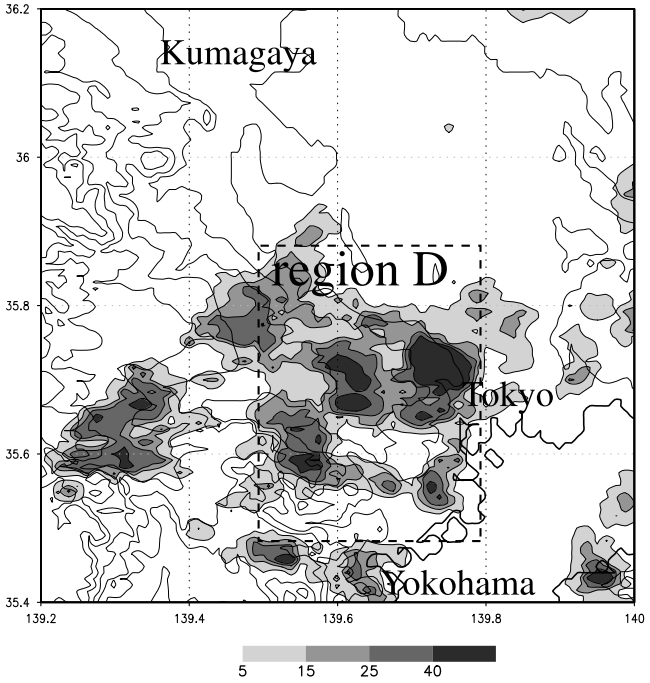

Figure 3. Three hour accumulated precipitation from 11:00 to 14:00 LST (02:00 to 05:00 UTC) on 5 August 2005 from radar-AMeDAS data over region B (shown in Figure 1). The thin solid contours denote terrain heights of 15, 30, 50, 80, 120, 200, and 300 m, and the thick solid contour indicates the terrain height of 0 m.

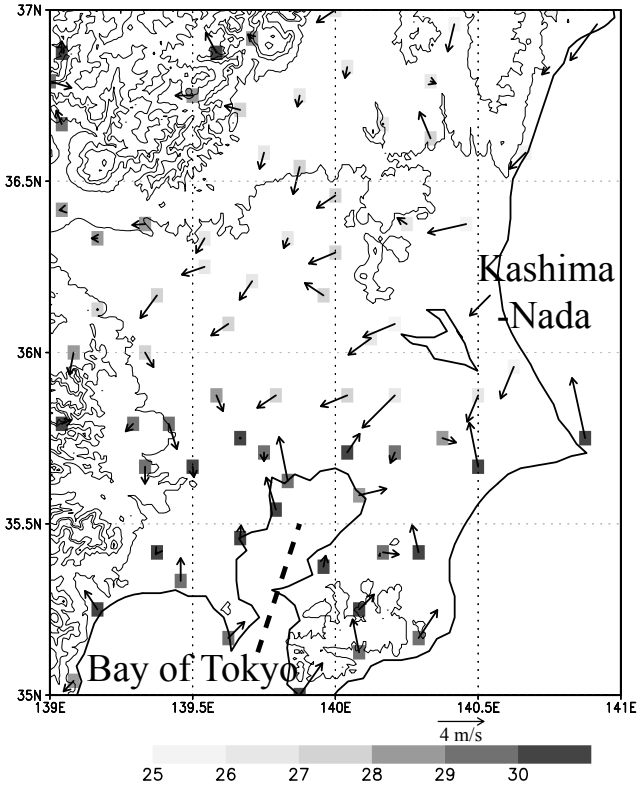

Figure 4. Surface wind and air temperature observed by the Automated Meteorological Data Acquisition System (AMeDAS) averaged from 10:00 to 11:00 LST (01:00 to 02:00 UTC) over region A in Figure 1. The values of air temperature were adjusted to the mean sea level. The contours have their meanings same as those in Figure 3.

model to assess the individual effects of artificial land cover and anthropogenic heat on a localized heavy rainfall event that occurred over Zoshigaya in Tokyo in 2008. The rest of the paper is organized as follows. The next section describes the numerical model used and the design of numerical experiments. The results are presented and discussed in section 3. Main conclusions are given in the last section.

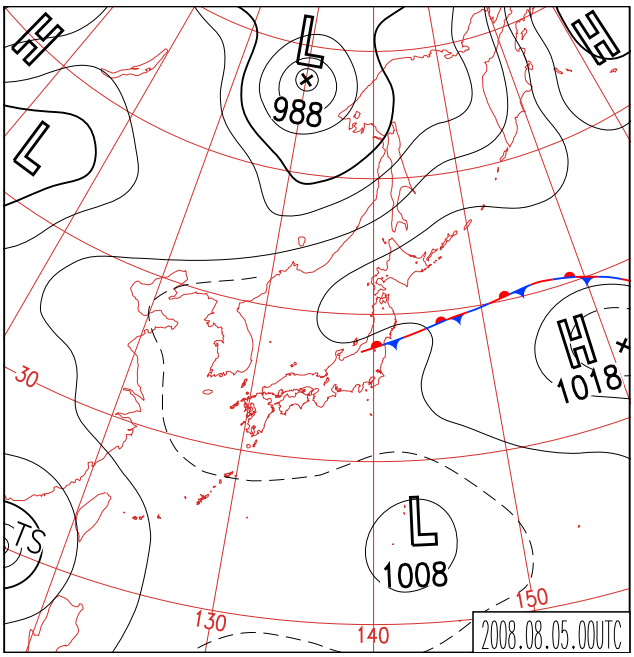

Figure 5. Surface weather map at 09:00 LST (00:00 UTC) on 5 August 2008.

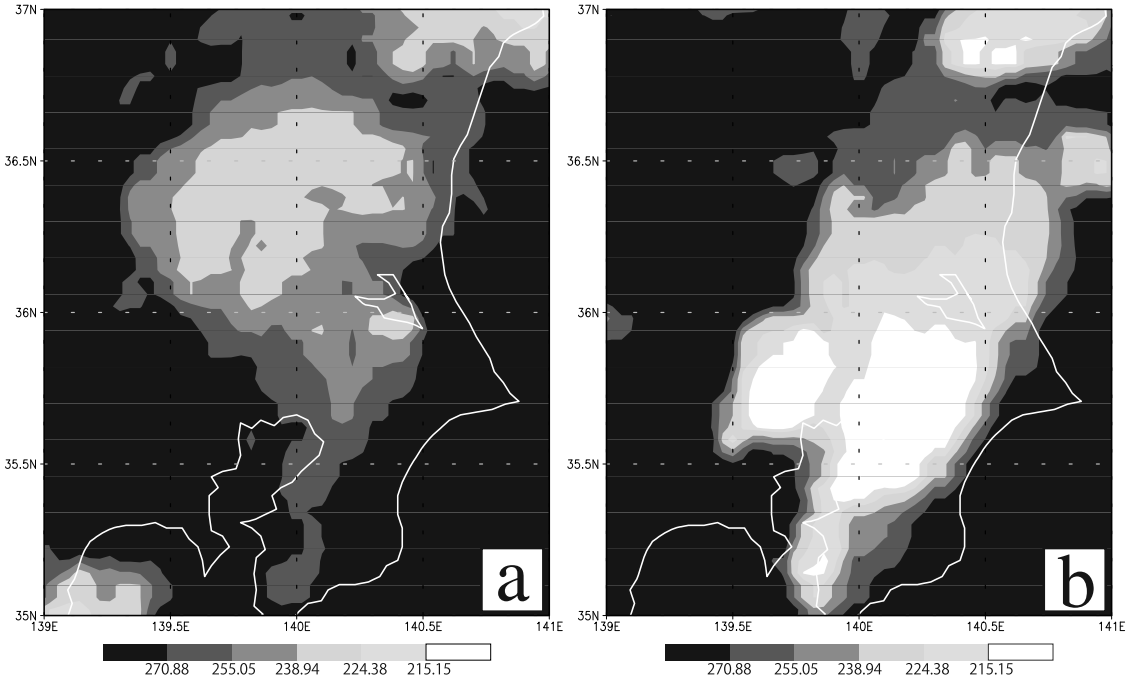

Figure 6. Images obtained by infrared channel 1 of the Multi-functional Transport Satellite (MTSAT) over Japan at (a) 10:00 LST (01:00 UTC) and (b) 13:00 LST (04:00 UTC).

2. Model Description and Experimental Design

2.1. Model Description

[10] In this study, the cloud-resolving model CReSiBUC (Cloud-Resolving storm simulator coupled with Simple Biosphere including Urban Canopy) [*Souma et al*., 2011, 2012, 2013; *Moteki et al*., 2005] was used. It consists of a nonhydrostatic meteorological model with high parallel computing efficiency, the Cloud-Resolving Storm Simulator (CReSS) [*Tsuboki and Sakakibara*, 2002], and an advanced land surface model including a realistic urban canopy scheme and irrigation scheme for cropland and the Simple Biosphere including Urban Canopy model (SiBUC) [*Tanaka*, 2004].

[11] The atmospheric model (CReSS) is based on nonhydrostatic and compressible equations in terrain-following coordinates. Prognostic variables include the three-dimensional velocity components, perturbations of pressure and potential temperature, water vapor mixing ratio, subgrid-scale turbulent kinetic energy, and cloud microphysical variables [*Tsuboki and Sakakibara*, 2002, 2007].

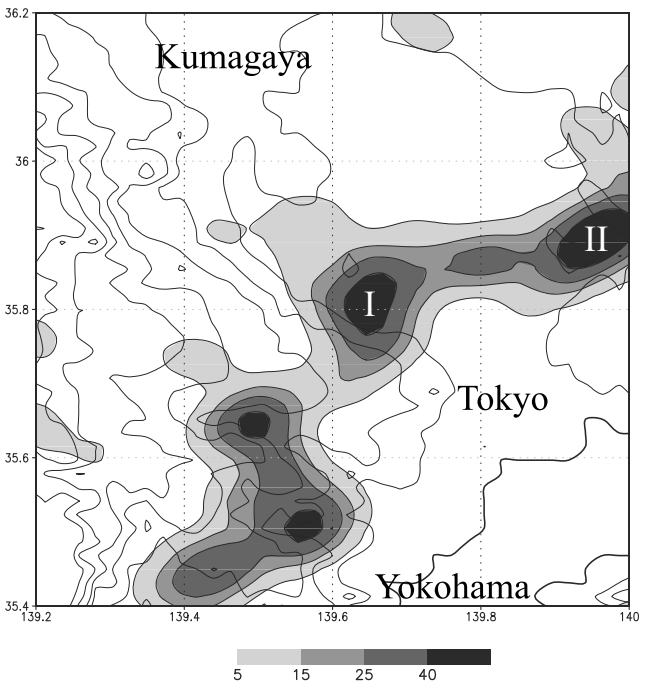

Figure 7. Three hour accumulated precipitation from 11:00 to 14:00 LST (02:00 to 05:00 UTC) on 5 August 2008 in the CTRL simulation over region B in Figure 1. The contours have their meanings the same as those in Figure 3.

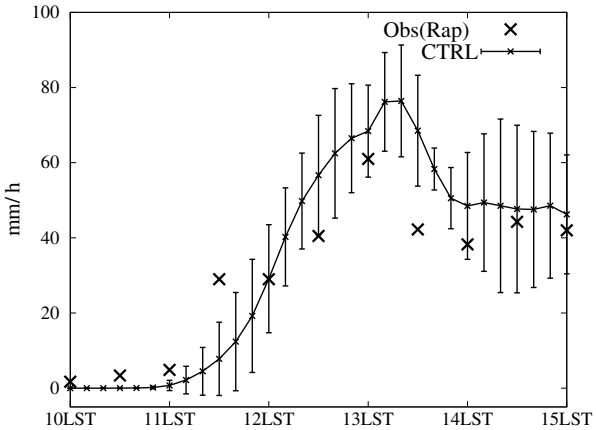

Figure 8. Time series of maximum hourly rainfall (mm h^{-1}) in region D (Figure 3). The curve represents the ensemble mean in the CTRL simulation, and the cross marks indicate observed values derived from radar-AMeDAS. The error bars indicate the ensemble standard deviation (spread) in CTRL.

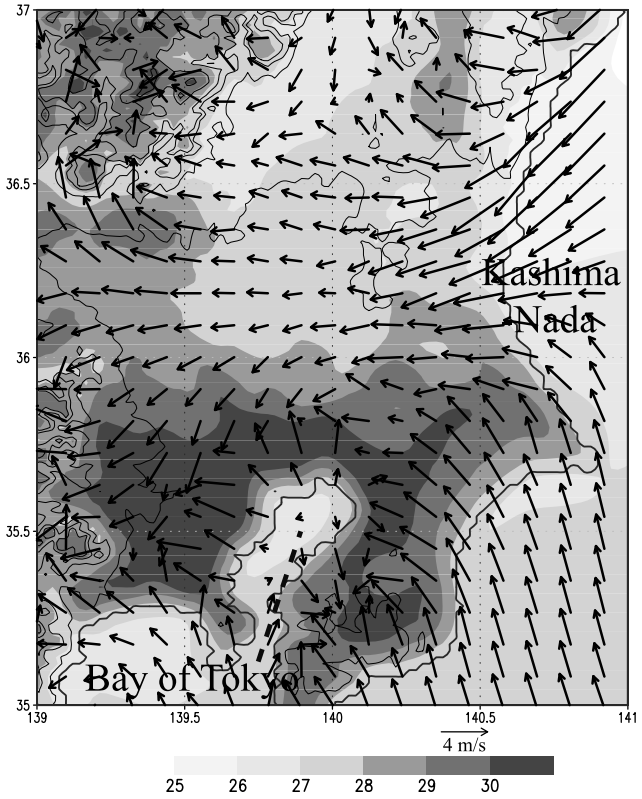

Figure 9. Surface wind and air temperature simulated in CTRL averaged from 10:00 to 11:00 LST (01:00 to 02:00 UTC) over region A in Figure 1. The values of air temperature were adjusted to the mean sea level. The contours have their meanings same as those in Figure 3.

[12] In CReSiBUC, the land surface model (SiBUC) calculates the radiation, heat, water, and momentum budgets, considering spatial and temporal land surface variations. The SiBUC model includes three submodels: the green area submodel, urban area submodel, and water body submodel. The SiBUC model calculates grid box-averaged surface fluxes by averaging the surface fluxes calculated in each submodel weighted by the fractional areas of green, urban, and water areas [*Tanaka*, 2004].

[13] Over urban areas, CReSiBUC considers the distribution of heat released from anthropogenic sources, including air conditioners and vehicles. CReSiBUC also considers the distribution of artificial land cover, including asphalt and geometrical structures, such as buildings of specific heights. CReSiBUC expresses the fraction of each building height within each grid box in the radiation and momentum budget calculations.

[14] The urban area submodel considers the puddles on roof, wall, and road surfaces. Their temperatures are assumed to be the same as those of roof, wall, and road surfaces. Only latent heat from puddles is considered in the heat budget of roof, wall, and road surfaces.

[15] The green area submodel is based on the Simple Biosphere Model 2 (SiB2) [*Sellers et al*., 1996] but includes some simplifications from the original SiB2. The green area submodel can consider artificial irrigation and drainage in rice paddy fields and other croplands [*Tanaka*, 2004].

[16] This study used a land use data set called KS-202, with a resolution of around 100 m, prepared by the Geographical Survey Institute (Government of Japan) to calculate the fractional areas of land use.

[17] The distribution of anthropogenic heat over urban areas was given based on data estimated by *Senoo et al.* [2004] and *Moriwaki et al*. [2008]. They multiplied the quantity of exhaust heat per unit area based on building use and automobile type by distributions, such as floor area and amount of traffic, and estimated the monthly average anthropogenic sensible heat distribution for any time of a day. To keep the comparison of the numerical experiments simple, anthropogenic latent heat was not considered in this study. The fraction of each building height, from 1 to 30 floors, within each grid box was estimated using a data set provided by the Metropolitan Tokyo Government Office.

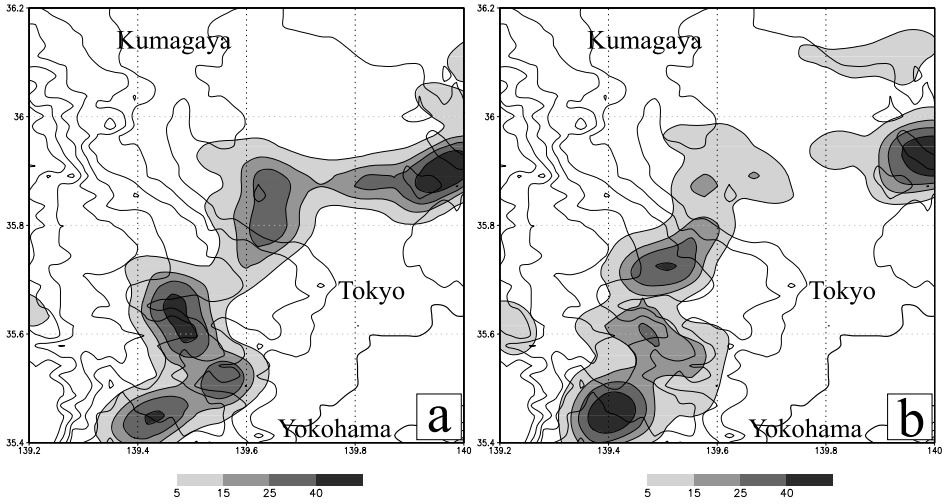

Figure 10. Three hour accumulated precipitation from 11:00 to 14:00 LST (02:00 to 05:00 UTC) on 5 August 2008 in region B in Figure 1 simulated in (a) NOAH and (b) NOLC. The contours have their meanings same as those in Figure 3.

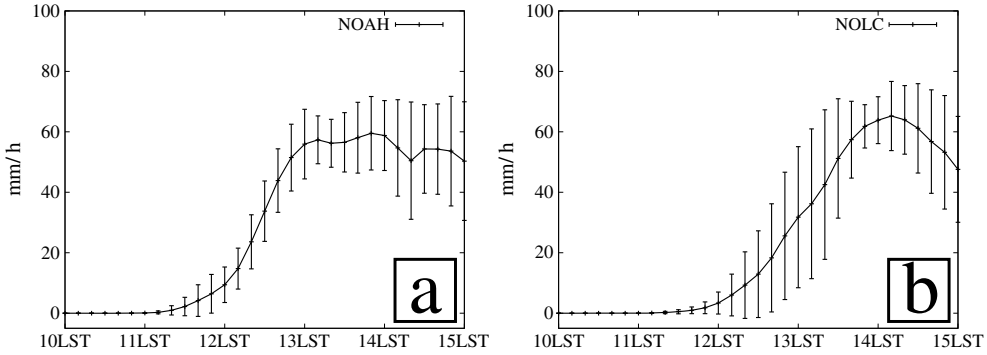

Figure 11. Time series of maximum hourly rainfall (mm h^{-1}) in region D (see Figure 3). The curve represents the ensemble mean in (a) NOAH and (b) NOLC. The error bars indicate the ensemble standard deviation (spread).

[18] The leaf area index in green areas was estimated using the normalized difference vegetation index for 10 day composite SPOT VEGETATION data (resolution of approximately 1 km) according to *Ebisu et al*. [2002]. Soil type was assigned by referring to a global digital soil map produced by the Food and Agricultural Organization of the United Nations, which has a resolution of approximately 10 km.

[19] The initial land surface temperature was assumed to be the same as the near-surface atmospheric temperature, and the initial soil moisture was set at a horizontally uniform wet condition (matric potential of −20 m). The NOAA/NASA Advanced Very High Resolution Radiometer Oceans Pathfinder monthly mean sea surface temperature (SST) data set [*Casey et al*., 2010], obtained from the U.S. National Oceanographic Data Center and the Group for High-Resolution SST, was used to give the model initial SST. This SST data set has a resolution of approximately 4 km.

[20] Realistic initial and lateral boundary conditions of the atmospheric variables were obtained from the mesoscale analysis (MANAL) of the Japan Meteorological Agency (JMA). Three-hourly MANAL data were interpolated linearly into hourly data.

[21] The bulk mixed-phase cloud microphysics scheme with the mixing ratios of cloud water, cloud ice, rainwater, snow, and graupel as prognostic variables was used for model moist physical processes [*Tsuboki and Sakakibara*, 2002, 2007]. A 1.5-order closure scheme with turbulent kinetic energy as a prognostic variable was used for subgrid-scale turbulent mixing processes [*Tsuboki and Sakakibara*, 2002, 2007]. The time interval of the large time step was set to be 3 s and that of the small time step was set to be 0.5 s.

[22] The model domain is shown in Figure 1 and the model atmosphere was discretized with a horizontal grid spacing of 2 km and 45 layers in the vertical (interval of approximately 300 m). The height of the lowest level of the model atmosphere was set to be 50 m to allow the lowest layer to be considered as the urban canopy layer can be treated in the urban area submodel. Note that a surface boundary layer including urban and vegetation canopy was calculated in the land surface model, and heat, water vapor, and momentum fluxes from the canopy layer were transferred to the atmospheric model. Although the lowest level of the model atmosphere is not low enough with sufficient near-surface vertical resolution to accurately simulate the nocturnal boundary layer and minimum temperature as indicated in *McNider et al*. [2012], it would not affect the main results of this study because the major concerns of this study are daytime convective boundary layer and maximum temperature.

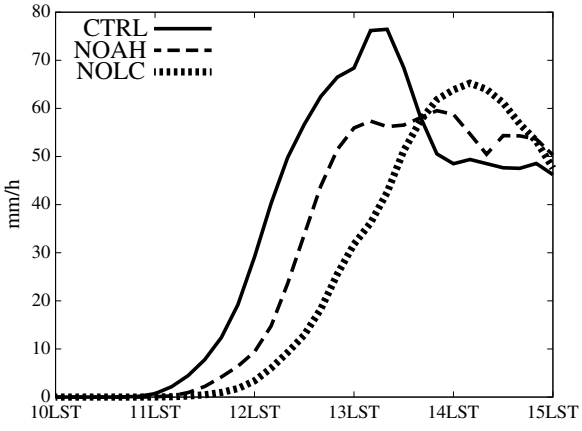

Figure 12. Time series of maximum hourly rainfall (mm h^{-1}) in region D (see Figure 3) for the ensemble mean in CTRL, NOAH, and NOLC.

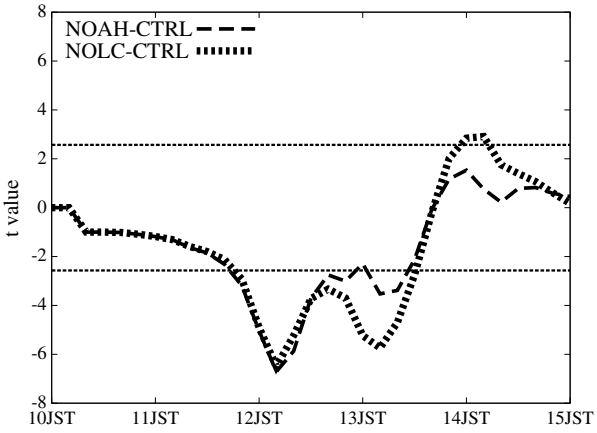

Figure 13. Time series of *t* value of maximum hourly rainfall in region D (see Figure 3) for the differences in the ensemble mean between NOAH and CTRL and between NOLC and CTRL. The horizontal dashed lines indicate the 95% confidence level (*t* value = 2.571 and −2.571).

Table 1. Terms of the Land Surface Energy Budget (Equation 1; W m^{-2}) Averaged From 10:00 LST (01:00 UTC) to 11:00 LST (02:00 UTC) and Averaged Over Region C in Figure 1

	CTRL	NOAH	NOLC
H_s	174.2	162.3	80.1
L_e	81.5	81.2	295.0
R_n	439.4	445.1	489.1
Q_m	20.0	0.0	20.0
G	203.6	221.7	134.0

2.2. Experimental Design

[23] CReSiBUC described above was used to conduct three ensemble experiments. The first experiment considered realistic land cover and urban features, including artificial land cover, anthropogenic heat, and urban geometry, and was referred to as CTRL. A schematic diagram of the heat budget for the land surface in CTRL is shown in Figure 2a. The second experiment (NOAH) considered the actual artificial land cover and urban geometry, but anthropogenic heat was ignored (as shown in Figure 2b). The third experiment (NOLC) also considered the actual artificial land cover and urban geometry but roofs, walls, and roads were replaced with shallow water of 0.1 mm deep to reduce urban heating from artificial land cover (as shown in Figure 2c). In a previous study, we carried out the no urban landscape experiment in which the urban area was replaced by rice paddy field [*Souma et al.*, 2013]. In that case, the effect of urban heating could not be isolated from that of urban geometry. To reduce only the heating from artificial land cover while keep the urban geometry, the NOLC experiment was designed in this study. Furthermore, because the focus of this study was on the different effects of urban heating, urban geometry (building height distribution) was prescribed.

[24] The land surface heat budget equation over an urban area can be written as

$$R_n + Q_m = G + H_s + L_e, \tag{1}$$

where R_n is the net radiation, Q_m is the anthropogenic heat, G is the ground heat flux, H_s is the surface sensible heat flux, and L_e is the surface latent heat flux. In NOAH, Q_m was ignored; therefore, H_s was expected to be lower over the urban area than in CTRL. In NOLC, the shallow water surface reduced surface heat flux as energy from solar radiation was used mostly for surface evaporation. However, the urban geometric shape (the building height distribution) and anthropogenic heat remained unchanged.

[25] Six members with initial conditions spanning 5 h from 02:00 to 07:00 local standard time (LST) on 5 August 2011 were carried out for each experiment as done in *Sen et al.* [2004]. The model was integrated continuously through 18:00 LST for each member run. To reduce the effect of chaotic behavior due to small differences in initial conditions, results of each experiment were considered in terms of the ensemble mean of the six member runs. For the spatial distribution of each physical quantity or the peak rainfall, the values of each ensemble member were averaged for each grid cell.

3. Results and Discussion

3.1. An Overview of the Localized Heavy Rainfall of 15 August 2008

[26] On 5 August 2008, four precipitation cells near Tokyo's Toshima Ward were monitored from 11:00 LST (02:00 UTC) to 14:00 LST (05:00 UTC) by the X-band multiparameter radar (MP-X) of the National Research Institute for Earth Science and Disaster Prevention, radar and surface rain gages of Japan Meteorology Agency (JMA) [*Kato and Maki*, 2009]. More than 80 mm of rainfall was recorded between 12:00 LST (03:00 UTC) and 13:00 LST

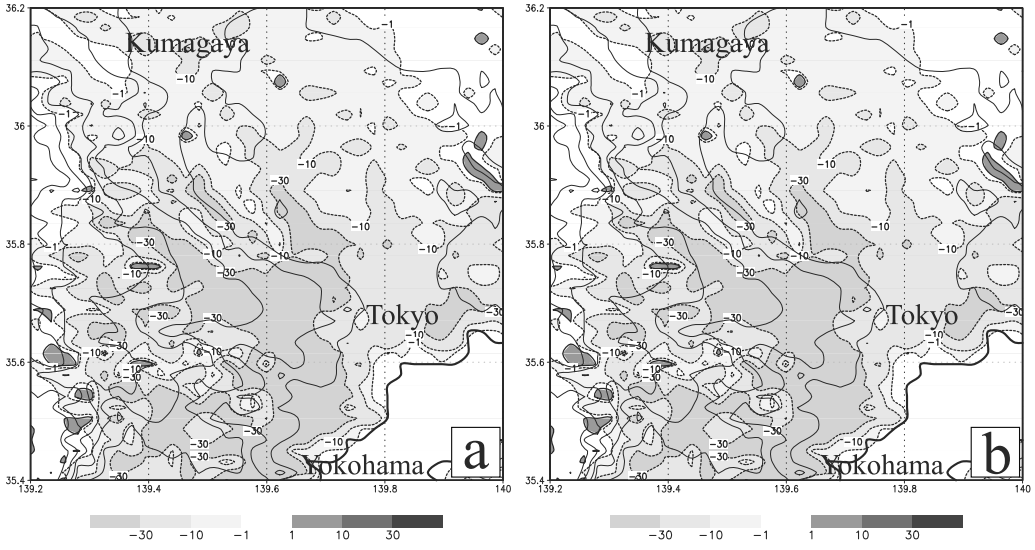

Figure 14. Differences in the ensemble means of sensible heat flux (W m^{-2}) (a) between NOAH and CTRL (NOAH–CTRL) and (b) between NOLC and CTRL (NOLC–CTRL) averaged from 07:00 to 08:00 LST (22:00 to 23:00 UTC) in region A (see Figure 1). Thick contours of −30, −10, and −1 W m^{-2} are shown in dash, and contours of 1, 10, and 30 W m^{-2} are shown in solid. The contours for terrain height are the same as those in Figure 3.

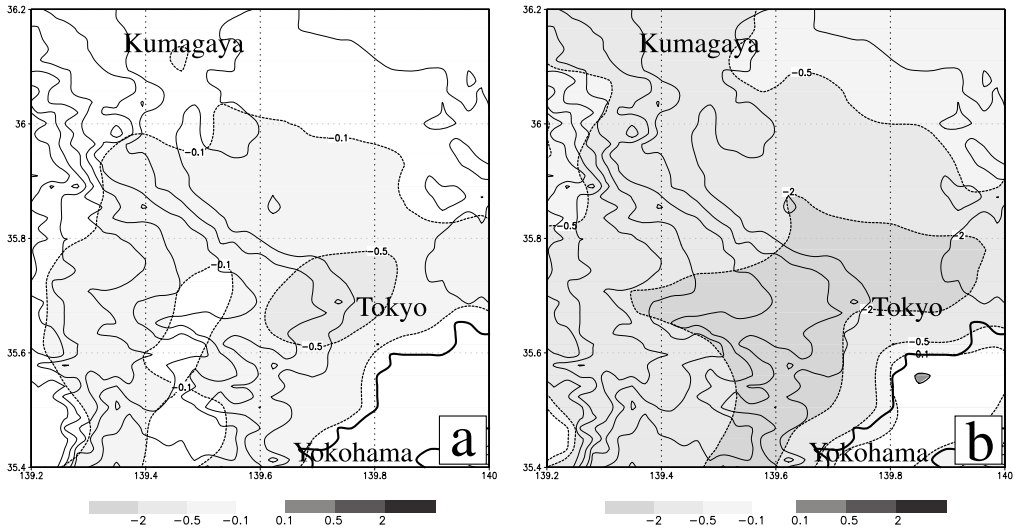

Figure 15. Differences in the ensemble means of near-surface air temperature (K) (a) between NOAH and CTRL (NOAH–CTRL) and (b) between NOLC and CTRL (NOLC–CTRL) averaged from 10:00 to 11:00 LST (02:00 to 03:00 UTC) in region A (see Figure 1). Contours of −2, −0.5, −0.1 K are shown in thick and dash, and contours of 0.1, 0.5, and 2 K are shown in solid. The contours for terrain height are the same as those in Figure 3.

(04:00 UTC) in a localized heavy rain area (about 5 km^2). Although the intensity was slightly smaller than that from MP-X, radar calibrated by AMeDAS rain gage data (radar-AMeDAS) provided by JMA (shown in Figure 3) also showed similar localized heavy rain areas.

[27] Figure 4 shows the averaged air temperature adjusted to the mean sea level and wind speed observed by AMeDAS between 10:00 LST (01:00 UTC) and 11:00 LST (02:00 UTC). Overall, the northeasterly wind from Kashima Nada prevailed. The northeasterly wind changed to the northerly wind near Tokyo due to the temperature difference between northern and southern Kanto and converged with wind from Tokyo Bay. This means that the horizontal wind convergence occurred prior to precipitation.

[28] Figures 5 and 6 show, respectively, the weather map and the infrared images taken from an infrared sensor of the Multi-functional Transport Satellite (MTSAT). A stationary front and the associated clouds were detected over northern Kanto at 10:00 LST (01:00 UTC) prior to precipitation (Figures 5 and 6). The cloud distribution was assumed to have suppressed temperature increase in northern Kanto, while temperature in southern Kanto relatively increased.

3.2. Precipitation Simulated in CTRL

[29] Figure 7 shows the 3 h accumulated precipitation from 11:00 LST (02:00 UTC) to 14:00 LST (05:00 UTC) simulated in CTRL. By comparing Figures 3 and 7, one can see that the intense precipitation area in Tokyo simulated in CTRL (precipitation area I in Figure 7) was slightly more inland than that observed. Furthermore, precipitation in Chiba (precipitation area II in Figure 7) appeared to the north of that observed (in analysis region B).

[30] The time series of the maximum hourly rainfall in region D, where intense precipitation was observed (Figure 3), is shown in Figure 8. The peak value of 76.4 mm h^{-1} was simulated from 12:20 LST (03:20 UTC) to 13:20 LST (04:20 UTC) in CTRL. According to the 2 km grid-averaged value of radar-AMeDAS, the peak rainfall of 61.0 mm h^{-1} occurred from 12:00 LST (03:00 UTC) to 13:00 LST (04:00 UTC). The peak value in CTRL was slightly larger than that observed and was delayed by about 20 min. Except for these discrepancies, the intense precipitation event in Tokyo was simulated reasonably well. Therefore, CTRL provided a reasonable representation of the time evolution of hourly maximum rainfall in Tokyo area. By comparing Figures 4 and 9, one can see that the CTRL simulation also reproduced the temperature difference between northern and southern Kanto and the convergence of the northerly wind in Tokyo with the southerly wind from Tokyo Bay.

3.3. Precipitation in Two Sensitivity Experiments

[31] As can be seen from Figures 7 and 10a, the localized heavy rainfall simulated over Tokyo (precipitation area I in Figure 7) in NOAH was weaker than that in CTRL and was clearly weakened and shifted westward in NOLC compared to that in CTRL (Figures 7 and 10b). As shown in Figures 10a and 10b, the reduction of precipitation was larger in NOLC than in NOAH.

[32] The time series of the maximum hourly rainfall in region D in each ensemble experiment is shown in Figures 11 and 12. The curve represents the ensemble mean, and the error bars indicate the standard deviation (spread) among the ensemble members. Although we used six ensemble members in this study, the ensemble standard deviation was not small and reflected the internal variability. Additionally,

Table 2. Precipitable Water (PW: kg m^{-2}) and Static Stability Index (SSI: K) Averaged From 10:00 LST (01:00 UTC) to 11:00 LST (02:00 UTC) Over Region C in Figure 1

	CTRL	NOAH	NOLC
PW	62.7	62.6	63.2
SSI	1.2	1.2	1.4

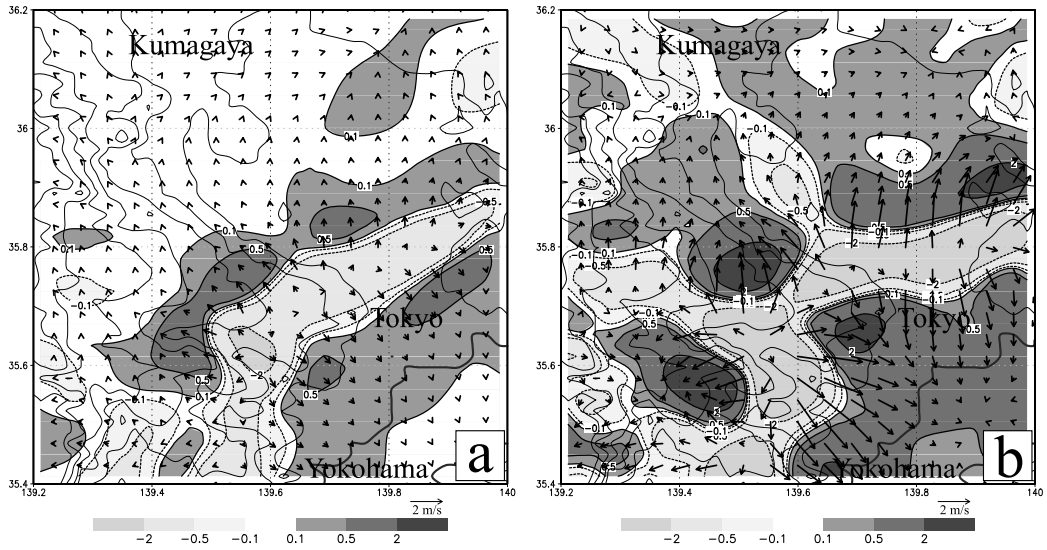

Figure 16. Differences in the ensemble means of horizontal wind convergence ($10^{-4}\,s^{-1}$) and near-surface wind speed ($m\,s^{-1}$) (a) between NOAH and CTRL (NOAH–CTRL) and (b) between NOLC and CTRL (NOLC–CTRL) averaged from 10:00 to 11:00 LST (02:00 to 03:00UTC) in region A (see Figure 1). Contours of −2, −0.5, and −0.1 are shown in thick and dash, and contours of 0.1, 0.5, and 2 are shown in solid. The contours for terrain height are the same as those in Figure 3.

compared with some previous studies using five ensemble members [e.g., *Sen et al.*, 2004], the six ensembles used in this study are marginally acceptable although more members could further improve the significance.

[33] The *t* test was carried out to detect the confidence level for the time series of maximum hourly rainfall in region D at every 10 min with *t* values shown in Figure 13. The difference in the time series of regional maximum hourly rainfall from 11:50 to 13:30 LST (02:50 to 04:30 UTC) except for 13:00 LST (04UTC) between CTRL and either NOAH or NOLC is statistically significant over 95% confidence level by the *t* test for each time interval (as shown in Figure 13).

[34] The maximum difference between NOAH and CTRL was −26.2 mm at 12:20 LST (03:20 UTC) and that between NOLC and CTRL was −44.2 mm at 12:40 LST (03:40 UTC). The averaged difference from 11:50 to 13:30 LST (except for 13:00 LST) between NOAH and CTRL was −19.2 mm and that between NOLC and CTRL was −33.8 mm. The results thus suggest that both anthropogenic heat and artificial land cover intensified precipitation and the effect of artificial land cover was larger than that of anthropogenic heat in this rainfall event. Note that in the middle stage of the precipitation event (13:30 LST; 04:30 UTC), the difference in area-averaged maximum hourly rainfall between NOAH and CTRL was −17.3 mm and that between NOLC and CTRL was −12.0 mm, suggesting that in the middle stage of the precipitation event, the difference between the two effects became small.

3.4. Effects of Anthropogenic Heat and Artificial Land Cover on Precipitation

[35] Table 1 shows the land surface heat budget averaged between 09:00 and 10:00 LST prior to precipitation, and Figure 14 shows the differences in sensible heat flux between NOAH and CTRL and between NOLC and CTRL, respectively. As expected, the sensible heat flux from land surface to the atmosphere was noticeably smaller in both NOAH and NOLC than in CTRL. Consistently, as shown in Figure 15, prior to precipitation, the temperature near the land surface of the urban area is lower in both NOAH and NOLC than in CTRL. In both NOAH and NOLC, the lower temperature over the urban area weakened both the northerly wind from the north and the southerly wind from Tokyo Bay toward Tokyo. As a result, the horizontal wind convergence and accompanying upward motion weakened in the urban area, resulting in relatively less precipitation in NOAH and NOLC, as shown in Figure 16.

[36] The differences in sensible heat flux, near-surface temperature, and surface wind convergence between NOAH and CTRL appeared in a more limited area over Tokyo than those between NOLC and CTRL. The differences in a more limited area between NOAH and CTRL resulted in a weaker effect on precipitation in NOAH than in NOLC in the early stage of the precipitation event. This is because high anthropogenic heat occurred in a limited area of Tokyo. As we can see from Table 1, the averaged effect of anthropogenic heat on sensible heat flux was smaller than that of artificial land cover.

[37] In the middle stage of the precipitation event, the effect of artificial land cover became weaker because the surfaces of artificial land cover became wetter and the incoming solar radiation became smaller due to the effect of clouds. In contrast, the effect of anthropogenic heat remained almost unchanged under the rainfall condition. These explain why the difference between the two effects became small in the middle stage of the precipitation event.

3.5. Associated Changes in Evaporation

[38] In NOLC, the decrease in sensible heat flux was also accompanied by substantial decreases in the amount of stored heat and upward longwave radiation because of the lower surface temperature. Since a large proportion of these energies were consumed by surface evaporation, the latent heat flux increased more in NOLC than in CTRL.

[39] Table 2 shows the Showalter stability index (SSI), which describes the static stability of the atmosphere and is defined as the difference between the temperature of an air parcel lifted adiabatically from 850 to 500 hPa and the actual temperature at 500 hPa. As seen from Table 2, although evaporation (latent heat flux) increased in NOLC, no significant differences were observed in precipitable water because of the reduced moisture convergence from the surroundings. In addition, surface temperature was lower in NOLC and thus, the atmosphere was more stable in NOLC than that in CTRL.

[40] Because Tokyo is located in the coastal region, changes in surface evaporation were mainly compensated by moisture convergence. As a result, changes in surface evaporation did not significantly affect precipitation for the studied case.

4. Conclusions

[41] This study investigated the respective effects of anthropogenic urban heat and artificial land cover on the localized heavy rainfall event occurred on 5 August 2008 in the Zoshigaya area of Tokyo's Toshima Ward. Three ensemble experiments were conducted: One experiment considered the actual urban features, the second experiment ignored only anthropogenic heat, and the third experiment reduced urban heating due to artificial land cover while kept the urban geometry unchanged.

[42] The results indicated that both anthropogenic heat and artificial land cover intensified precipitation, significant over 95% confidence level as detected by *t* test. The rainfall event examined in this study was quite similar to that studied by *Matheson and Ashie* [2008], who reported a strong urban effect on rainfall amount over the urbanized area (both events occurred over the heavily urbanized area of Tokyo). The effect of artificial land cover in this study was greater than that of anthropogenic heat in the early stage of precipitation. However, in the middle stage of the precipitation event, the difference between the two effects became small.

[43] In the experiment with decreased urban heating, the decrease in precipitation was mainly related to the lower surface temperature of the urban area and the weakened horizontal wind convergence and the associated upward motion. The smaller sensible heat flux, near-surface temperature, and surface wind convergence, seen in a more limited area, resulted in a weaker effect on precipitation in NOAH than in NOLC in the early stage of precipitation. This is because high anthropogenic heat only occurred in a limited area of Tokyo and the average effect of anthropogenic heat on sensible heat flux was smaller than that of artificial land cover.

[44] In the middle stage of the precipitation event, the effect of artificial land cover weakened because the surfaces of artificial land cover became wet due to precipitation and the incoming solar radiation was reduced by clouds. In contrast, the effect of anthropogenic heat remained almost unchanged even under the rainfall condition. These explain why the difference between the two effects became small in the middle stage of the precipitation event.

[45] In addition to the effect of urban heating, the effects of urban geometry [e.g., *Ryu and Baik*, 2012] and enhanced aerosols serving as cloud condensation nuclei in the urban environment [e.g., *van den Heever and Cotton*, 2007] on urban weather and climate have also been reported. These additional effects could be compared with the effects of anthropogenic heat and artificial land cover examined in this study in future work. In this study, ensemble experiments were utilized to assess the urban effect. However, only six members for each experiment were conducted. In future studies, more ensemble members and higher spatial resolution can be used to enhance the robustness of the findings and to achieve improved simulations. In addition, multiple case studies will also be helpful for clarifying conditions under which the effects of anthropogenic heat and artificial land cover become more important than other unban environmental conditions, as investigated in *Matheson and Ashie* [2008].

[46] **Acknowledgments.** The authors thank Manabu Kanda and Hiroshi Senoo (Tokyo Institute of Technology) and Ryo Moriwaki (Ehime University) for providing the anthropogenic heat data sets. We also thank Hiroshi Ishidaira, Yutaka Ichikawa, Jun Magome (University of Yamanashi), and Kei Yoshimura (University of Tokyo) for helpful discussions. The geometric structure data set was provided by the Metropolitan Tokyo Government Office. This study was supported by the Special Coordination Funds for Promoting Science and Technology, the Global COE Program of the University of Yamanashi, grants (A) 22246066 and (S) 22226010, and grants for Young Researcher (B) 24760390 from the Ministry of Education, Culture, Sports, Science and Technology (MEXT), Japan. This study was also supported by JAMSTEC through its sponsorship of the International Pacific Research Center (IPRC) at the School of Ocean and Earth Science and Technology (SOEST) at the University of Hawaii.

References

Casey, K. S., T. B. Brandon, P. Cornillon, and R. Evans (2010), The past, present and future of the AVHRR pathfinder SST program, in *Oceanography From Space: Revisited*, edited by V. Barale, J. F. R. Gower, and L. Alberotanza, pp. 273–287, Springer, Dordrecht, The Netherlands, doi:10.1007/978-90-481-8681-5_16.

Changnon, S. A., Jr., and F. A. Huff (1986), The urban-related nocturnal rainfall anomaly at St. Louis, *J. Appl. Meteorol. Climatol.*, *25*, 1985–1995.

Ebisu, N., A. Nishikawa, A. Kondo, E. Nakakita, and K. Tanaka (2002), Study on seasonal variations of NDVI, LAI and evapotranspiration in forest, Proceedings of the 3rd Workshop for Remote Sensing of Hydrological Processes and Its Applications, 59–65.

Fujibe, F. (1998), Spatial anomalies and long-term changes of precipitation in Tokyo, *Teknki*, *45*, 7–18 (in Japanese with English abstract).

Gero, A. F., and A. J. Pitman (2006), The impact of land cover change on a simulated storm event in the Sydney basin, *J. Appl. Meteorol. Climatol.*, *45*, 283–300.

Kanda, M., Y. Inoue, and I. Ito (2001), Numerical study on cloud lines over an urban street in Tokyo, *Boundary Layer Meteorol.*, *98*, 251–273.

Kanda, M., T. Kawai, M. Kanega, R. Moriwaki, K. Narita, and A. Hagishima (2005), Simple energy balance model for regular building arrays, *Boundary Layer Meteorol.*, *116*, 423–443.

Kato, A., and M. Maki (2009), Localized heavy rainfall near Zoshigaya, Tokyo, Japan on 5 August 2008 observed by X-band polarimetric radar—Preliminary analysis, *SOLA*, *5*, 89–92, doi:10.2151/sola.2009-023.

Kawabata, T., H. Seko, K. Saito, T. Kuroda, K. Tamiya, T. Tsuyuki, Y. Honda, and Y. Wakazuki (2007), An assimilation and forecasting experiment of the Nerima heavy rainfa11 with a cloud-resolving nonhydrostatic 4-dimensional variational data assimilation system, *J. Meteorol. Soc. Jpn.*, *85*, 255–276.

Kishtawal, C. M., D. Niyogi, M. Tewari, R. A. Pielke Sr., and J. M. Shepherd (2009), Urbanization signature in the observed heavy rainfall climatology over India, *Int. J. Climatol.*, *30*, 1908–1916, doi:10.1002/joc.2044.

Kusaka, H., and F. Kimura (2004), Coupling single-layer urban canopy model with a simple atmospheric model: Impact on urban heat island simulation for an idealized case, *J. Meteorol. Soc. Jpn.*, *82*, 67–80.

Kusaka, H., H. Kondo, Y. Kikegawa, and F. Kimura (2001), A simple single-layer urban canopy model for atmospheric models: Comparison with multi-layer and slab models, *Boundary Layer Meteorol.*, *101*, 329–358.

Lei, M., D. Niyogi, C. Kishtawal, R. Pielke Sr., A. Beltran-Przekurat, T. Nobis, and S. Vaidya (2008), Effect of explicit urban land surface representation on the simulation of the 26 July 2005 heavy rain event over Mumbai, India, *Atmos. Chem. Phys. Discuss.*, *8*, 8773–8816.

Matheson, M. A., and Y. Ashie (2008), The effect of changes of urban surfaces on rainfall phenomenon as determined by a non-hydrostatic mesoscale model, *J. Meteorol. Soc. Jpn.*, *86*, 733–751.

McNider, R. T., G. J. Steeneveld, B. Holtslag, R. Pielke Sr, S. Mackaro, A. Pour Biazar, J. T. Walters, U. S. Nair, and J. R. Christy (2012), Response and sensitivity of the nocturnal boundary layer over land to added longwave radiative forcing, *J. Geophys. Res.*, *117*, D14106, doi:10.1029/2012JD017578.

Moriwaki, R., H. Senoh, M. Kanda, A. Hagishima, and T. Kinouchi (2008), Anthropogenic water vapor emissions in Tokyo, *Water Resour. Res.*, *44*, W11424, doi:10.1029/2007WR006624.

Moteki, Q., Y. Ito, K. Yorozu, K. Souma, A. Sakakibara, K. Tsuboki, T. Kato, K. Tanaka, and S. Ikebuchi (2005), Estimation for effects of existence of urban on development of cumulonimbus clouds using atmosphere-land coupled model of CReSiBUC, *Annu. Disast. Prev. Res. Inst., Kyoto Univ.*, *48C*, 197–208.

Niyogi, D., P. Pyle, M. Lei, S. P. Arya, C. M. Kishtawal, M. Shepherd, F. Chen, and B. Wolfe (2010), Urban modification of thunderstorms: An observational storm climatology and model case study for the Indianapolis urban region, *J. Appl. Meteorol. Climatol.*, *50*, 1129–1144.

Pielke, R. A., Sr., J. Adegoke, A. Beltran-Przekurat, C. A. Hiemstra, J. Lin, U. S. Nair, D. Niyogi, and T. E. Nobis (2007), An overview of regional land-use and land-cover impacts on rainfall, *Tellus B*, *59*, 587–601.

Pielke, R. A., Sr., et al. (2011), Land use/land cover changes and climate: Modeling analysis and observational evidence, *WIREs Clim. Change*, *2*(6), 828–850, doi:10.1002/wcc.144.

Ryu, Y.-H., and J.-J. Baik (2012), Quantitative analysis of factors contributing to urban heat island intensity, *J. Appl. Meteorol. Climatol.*, *51*, 842–854.

Sato, T., T. Terashima, T. Inoue, and F. Kimura (2006), Intensification of convective precipitation system over Tokyo urban area in summer season, *Tenki*, *56*, 479–484 (in Japanese with English abstract).

Sellers, P. J., D. A. Randall, G. J. Collatz, J. A. Berry, C. B. Field, D. A. Dazlich, C. Zhang, G. D. Collelo, and L. Bounoua (1996), A revised land surface parameterization (SiB2) for atmospheric GCMs. Part I: Model formulation, *J. Clim.*, *9*, 676–705.

Sen, O. L., Y. Wang, and B. Wang (2004), Impact of Indochina deforestation on the East Asian Summer Monsoon, *J. Clim.*, *17*, 1366–1380.

Senoo, H., M. Kanda, T. Kinouchi, and A. Hagishima (2004), Estimation of anthropogenic heat and vapor emission and the impact of regional urban climate, *Annu. J. Hydraul. Eng.*, *48*, 169–174 (in Japanese with English abstract).

Shem, W., and J. M. Shepherd (2009), On the impact of urbanization on summertime thunderstorms in Atlanta: Two numerical model case studies, *Atmos. Res.*, *92*, 172–189.

Shepherd, J. M. (2005), A review of current investigations of urban-induced rainfall and recommendations for the future, *Earth Interact.*, *9*, 1–27.

Shepherd, J. M., and S. J. Burian (2003), Detection of urban-induced rainfall anomalies in a major coastal city, *Earth Interact.*, *7*, 1–17.

Shepherd, J. M., M. Carter, M. Manyin, D. Messen, and S. Burian (2010), The impact of urbanization on current and future coastal precipitation: A case study for Houston, *Environ. Plann.*, *37B*, 284–304.

Souma, K., K. Sunada, T. Suetsugi, and K. Tanaka (2011), The effect of urban area on a heavy rainfall event over Tokyo on August 5 2008, Preprints, International Conference on MCSs and High-Impact Weather, Nagoya, Japan, Japan Meteorological Society and Nagoya University, 353–356.

Souma, K., K. Tanaka, K. Sunada, T. Suetsugi, K. Tsuboki, A. Sakakibara, and Q. Moteki (2012), The effect of urban heating on a localized heavy rainfall near Zoshigaya in Tokyo in 2008, *Annu. J. Hydraul. Eng., JSCE*, *56*, 403–408 (in Japanese with English Abstract).

Souma, K., K. Sunada, T. Suetsugi, and K. Tanaka (2013), Use of ensemble simulations to evaluate the urban effect on a localized heavy rainfall event in Tokyo, Japan, *J. Hydro. Environ. Res.*, doi:10.1016/j.jher.2013.05.001.

Tanaka, K. (2004), Development of the new land surface scheme SiBUC commonly applicable to basin water management and numerical weather prediction model. PhD dissertation, Kyoto University.

Tanaka, K., and S. Ikebuchi (1994), Simple biosphere model including urban canopy (SiBUC) for regional or basin-scale land surface processes, Proceedings of the International Symposium on GEWEX Asian Monsoon Experiment, Beijing, China, Peking University, 59–62.

Tsuboki, K., and A. Sakakibara (2002), in *Large-Scale Parallel Computing of Cloud Resolving Storm Simulator, High Performance Computing*, edited by H. P. Zima et al., pp. 243–259, Springer, Germany.

Tsuboki, K., and A. Sakakibara (2007), Numerical prediction of high-impact weather systems, Seventeenth International Hydrological Program (IHP) Training Course, 246 pp.

van den Heever, S. C., and W. R. Cotton (2007), Urban aerosol impacts on downwind convective storms, *J. Appl. Meteorol. Climatol.*, *46*, 828–850.